J. Fluid Mech. (2003), *vol.* 493, *pp.* 255–275.
DOI: 10.1017/S0022112003005901 Printed in the United Kingdom

On fine sediment transport by long waves in the swash zone of a plane beach

By DAVID PRITCHARD[1] AND ANDREW J. HOGG[2]

[1]BP Institute for Multiphase Flow, University of Cambridge, Madingley Rise, Madingley Road, Cambridge CB3 0EZ, UK

[2]Centre for Environmental and Geophysical Flows, School of Mathematics, University of Bristol, University Walk, Bristol BS8 1TW, UK

(Received 2 September 2002 and in revised form 11 March 2003)

We calculate suspended sediment transport, erosion and deposition under reflected long waves on a plane beach. Our method employs the shallow-water equations, and is based on the calculation of the concentration field in Lagrangian coordinates: this allows results to be obtained readily throughout the whole domain, including the often troublesome shoreline region. These results suggest that the tendency of wave-dominated muddy shores to export sediment and erode over long time scales is not due to wave forcing at infragravity frequencies, since the sediment transport under such waves is localized close to the shoreline, and is principally directed shorewards. They also provide easily reproduced test cases against which to validate the numerical methods used in more detailed studies of coastal sediment transport and morphodynamics.

1. Introduction

In recent years the morphodynamics of intertidal mudflats have emerged as a subject of considerable interest within the coastal engineering community. These extensive gently sloping shores are found throughout the world, wherever there is a sufficient supply of fine sediment (Flemming 2002); they are an especially important environment along the coasts of north-western Europe, including the British Isles, where they dominate the shores of many estuaries. Mudflats are ecologically important because they provide a habitat for many species of wading birds which feed on the microfauna within the top layers of the mud, while they are of interest to the engineer for the contribution they make to coastal defence, and as a substantial sink or source of sediment when contemplating large-scale works such as barrages or channel dredging.

The morphology and the long-term behaviour of muddy intertidal systems are principally governed by the relative importance of tidal currents and wind-generated waves in mobilizing and transporting sediment (Dyer 1998; Kirby 2000; Le Hir *et al.* 2000). Of these mechanisms, tidal currents are the better understood, and have been the subject of several recent analytical and numerical studies (Friedrichs & Aubrey 1996; Roberts, Le Hir & Whitehouse 2000; Pritchard, Hogg & Roberts 2002; Pritchard & Hogg 2003). The role of waves is rather less well understood, and although recent studies have investigated their effects both in isolation (e.g. Friedrichs & Aubrey 1996; Lee & Mehta 1997) and in conjunction with tidal currents

(Roberts *et al.* 2000; Rodriguez & Mehta 2001), the greater complexity of the hydrodynamics means that the models employed are necessarily more heuristic, and the transport processes involved are generally less well understood.

Field observations (e.g. Whitehouse & Mitchener 1998; Christie, Dyer & Turner 1999; Dyer *et al.* 2000; Janssen-Stelder 2000) suggest that waves contribute to sediment transport in three ways: by increasing bed shear stresses and thus the rate at which sediment is entrained into the water column; by mixing and transporting sediment which is already suspended; and by breaking up the top layer of the muddy bed so that it flows seawards under gravity as a layer of fluid mud. The net effect of these processes is generally to erode sediment from the flats and export it seawards; however, the relative importance of the processes, and the interactions between them, are not well understood. There is therefore a need for studies which examine these processes separately, with the aim of providing understanding which can inform the development of more complete simulations.

In the current paper, we consider one such process. The hydrodynamics in the swash zone of a gently sloping beach are often dominated by the non-breaking low-frequency motions generally referred to as infragravity waves (see for example Baldock & Holmes 1999). These may be refractively trapped by longshore currents to form edge waves, or reflected seawards ('leaky' waves). The influence which either form of infragravity motion has on the morphodynamics of the swash and surf zone remains uncertain, although both have been discussed as possible explanations for morphological features on sandy beaches (Holman & Sallenger 1993; Komar 1998). Their role as agents of sediment transport on beaches and flats dominated by finer cohesive material has received rather less attention.

To investigate this role, we consider 'leaky' waves on a flat or beach with a linear cross-shore profile. Although this linear profile is an idealization of the shape of real flats, which may range from concave- to convex-upwards depending on the hydrodynamic regime and long-term erosional trends (Kirby 2000), it provides a useful model for investigating sediment transport processes. It also offers a considerable advantage from the point of view of analysis, in that long-wave motions may be investigated within a shallow-water model using the formalism developed by Carrier & Greenspan (1958).

In this formalism, the governing partial differential equation for suspended sediment transport may be reduced, by considering transport in Lagrangian coordinates, to a system of ordinary differential equations which are easily integrated numerically by standard methods. This allows highly accurate numerical results to be obtained with considerably greater ease and accuracy than by directly integrating the partial differential equation. In particular, it resolves the problems which numerical methods commonly encounter in representing the flow and sediment transport near the moving shoreline. Indeed, a secondary motivation of the work described here is the development of easily reproduced 'test-bed' solutions for sediment transport which may be used to validate the sediment transport routines which are employed in numerical studies of coastal sediment transport and morphodynamics over less idealized bathymetries.

We consider both the basic solution for a monochromatic standing wave derived by Carrier & Greenspan (1958) and a class of bimodal oscillations formed by superimposing these basic solutions. The first of these is of particular interest from the point of view of model validation, as it has long been a standard test case for numerical models of the nearshore region (see, for example, Hibberd & Peregrine 1979; Vincent, Caltagirone & Bonneton 2001). The second provides insight into the

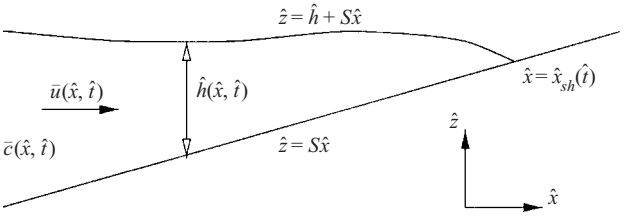

FIGURE 1. Geometry of the cross-shore model.

interaction of nearby modes which may be expected to influence transport under a more complex spectrum of wave energy.

The prototypical form of sediment considered in this paper is fine cohesive sediment which possesses a threshold shear stress for erosion and may also posess a critical shear stress for deposition; however, the approach may easily be adapted to consider other types of sediment with different models for the erosion and deposition fluxes. Indeed, we are able to demonstrate that our results are qualitatively unaffected by quite large variations in the expressions which describe the erosion and deposition of sediment.

In § 2, we describe the models employed for the hydrodynamics and the erosion, deposition and transport of sediment. In § 3 we present Carrier & Greenspan's formalism for describing the hydrodynamics on a plane beach, along with the basic solution for a reflected wave, and cast this in Lagrangian form. In §§ 4 and 5, we construct periodic solutions for sediment transport under monochromatic and bichromatic oscillations: we present them and discuss them in both Lagrangian and Eulerian frames, with particular reference to transport patterns close to the shoreline (the swash zone). Finally, in § 6 we summarize our findings and discuss their application to the problem of sediment transport on intertidal flats.

2. The shallow-water model

The geometry of our model is shown in figure 1. We consider purely cross-shore flow, and we make the standard shallow-water approximation (Peregrine 1972) based on the assumption that the characteristic horizontal length scale of the flow is much greater than the characteristic vertical length scale. This is readily justified for flows on wave-dominated flats, for which typical gradients are of the order of $1/100$ (see, for example, O'Brien, Whitehouse & Cramp 2000). Under this assumption, the pressure may be shown to be hydrostatic to leading order, and the flow may be described in terms of the fluid depth $\hat{h}$ and a depth-averaged horizontal velocity $\bar{u}$. (Here and elsewhere, both carets and overbars denote dimensional quantities, and dimensionless quantities are unadorned.)

Fluid continuity is then expressed as

$$\frac{\partial \hat{h}}{\partial \hat{t}} + \frac{\partial}{\partial \hat{x}}(\bar{u}\hat{h}) = 0, \tag{2.1}$$

while the conservation of momentum, when boundary shear stresses are neglected, has the form

$$\frac{\partial \bar{u}}{\partial \hat{t}} + \bar{u}\frac{\partial \bar{u}}{\partial \hat{x}} = -\hat{g}\frac{\partial \hat{h}}{\partial \hat{x}} - \hat{g}S. \tag{2.2}$$

Here $\hat{g}$ is the acceleration due to gravity, and S represents the slope of the bed. We are concerned throughout this paper with flow for which S is a constant, so the surface elevation is given by $\hat{h} + S\hat{x}$.

We are generally concerned with relatively gentle flows, over the rather smooth beds typical of fine cohesive sediment (Dyer 1986), and so we neglect the effects of friction throughout. This neglect follows the success of frictionless shallow-water models in describing many aspects of nearshore hydrodynamics, in many studies over the last fifty years (see, for example, Peregrine 1972; Barnes 1996; Carrier, Wu & Yeh 2003). Formally, this neglect means that our model is invalid in the near vicinity of the shoreline, where frictional terms become comparable to inertial ones, and that caution must be applied in interpreting our results. However, the success of the purely hydrodynamic studies offers some encouragement that such frictionless models can capture the essential features of the dynamics of the nearshore region.

The shallow-water equation for the conservation of sediment transported as a dilute, well-mixed suspension is

$$\frac{\partial \bar{c}}{\partial \hat{t}} + \bar{u}\frac{\partial \bar{c}}{\partial \hat{x}} = \frac{\hat{q}_e - \hat{q}_d}{\hat{h}}, \tag{2.3}$$

where $\bar{c}$ represents the depth-averaged mass concentration of suspended sediment, and $\hat{q}_e$ and $\hat{q}_d$ are, respectively, the mass erosion and mass deposition fluxes which represent exchanges between the water column and the bed.

Implicit in this expression is the assumption that the flow is fully turbulent and that the turbulent mixing is sufficient that sediment is well-mixed vertically in the water column. The thickness of the turbulent boundary layer under oscillatory flow may be shown (Dyer 1986) to scale as $\hat{\delta} = \hat{u}_*/\hat{\omega}$, where $\hat{\omega}$ is the angular frequency of the motion and $\hat{u}_*$ is a friction velocity defined in terms of the bed shear stress $\hat{\tau}_b$ by $\hat{\rho}\hat{u}_*^2 = \hat{\tau}_b$. For waves of the kind considered here, with periods of the order of 100 s, and typical maximum bed shear stresses $\hat{\tau}_b = 0.7\,\mathrm{N\,m^{-2}}$, the thickness $\hat{\delta}$ is of the order of 0.5 m. We will, however, treat the turbulent layer as extending throughout the water column. This is a severe assumption, and we note the possibility that there may be a systematic contribution to sediment transport arising from a time-dependent vertical flow structure and from the vertical distribution of sediment, as in other coastal situations (Bass *et al.* 2002). However, it is a valuable simplification because it makes the problem substantially more amenable to analysis.

Under this assumption, the vertical distribution of sediment may be characterized by the Rouse number for vertical mixing, $B = \hat{w}_s/(\kappa\hat{u}_*)$, where $\hat{w}_s$ is a particle settling velocity and κ is the von Kármán constant. Taking a typical value of $\hat{w}_s = 1\,\mathrm{mm\,s^{-1}}$, we obtain $B \approx 0.1$, which is sufficiently small for stratification to be neglected at leading order.

In general, $\hat{q}_e$ and $\hat{q}_d$ are functions of $\bar{u}$ and of $\bar{c}$. In the present study, we employ a standard formula for the erosion of cohesive sediment,

$$\hat{q}_e = \begin{cases} \hat{m}_e\left(\dfrac{\bar{u}^2}{\hat{u}_e^2} - 1\right) & \text{for } |\bar{u}| \geqslant \hat{u}_e, \\ 0 & \text{for } |\bar{u}| < \hat{u}_e, \end{cases} \tag{2.4}$$

where $\hat{m}_e$ is a constant with the dimensions of mass flux per unit area of the bed. This model was obtained experimentally (see Sanford & Maa 2001), and is commonly used to describe the erosion of sediment from a cohesive bed, where some critical shear stress, corresponding to a velocity $\hat{u}_e$, must be exceeded in order to break up the bed and entrain particles. Models of the erosion of non-cohesive sediment often have

a similar form, though they are typically proportional to the quantity $(\bar{u}^2/\hat{u}_e^2 - 1)^n$, where the exponent n lies in the range $3/2 \leqslant n \leqslant 7/2$ (Dyer & Soulsby 1988).

The deposition of fine suspended sediment is a complex process, which is controlled largely by the formation and break-up of large particle aggregates (flocs), and there is as yet no complete model which can describe these processes on the basis of the small-scale physics. However, the empirical description due to Einstein & Krone (1962), in which deposition occurs only when the near-bed shear stresses are sufficiently small for flocs to reach the bed without being broken up and re-entrained, is almost universally employed to describe the deposition of muddy sediment in estuarine and coastal environments (Dyer 1986; Krone 1993).

In the current study, we employ the modification of this description which was proposed by Pritchard & Hogg (2003). In this model, most mud in suspension is deposited as flocs with a characteristic settling velocity $\hat{w}_s$. However, at high shear rates flocs may be broken up by near-bed turbulence into much smaller primary particles, with settling velocity $\hat{w}_p$. We then model the depositional flux as

$$\hat{q}_d = \begin{cases} \hat{w}_p \bar{c} & \text{for } |\bar{u}| > \hat{u}_d, \\ \hat{w}_s \bar{c} \left(1 - (1-\epsilon)\dfrac{\bar{u}^2}{\hat{u}_d^2}\right) & \text{for } |\bar{u}| \leqslant \hat{u}_d, \end{cases} \tag{2.5}$$

where $\epsilon = \hat{w}_p/\hat{w}_s$. This reduces in the limit $\epsilon = 0$ to the model due to Einstein & Krone (1962), while in the alternative limit $\epsilon = 1$, it reduces to the continuous deposition of particles, which would be appropriate for non-cohesive sediment. The advantage of employing $\epsilon > 0$ to describe fine sediment deposition is partly conceptual, in that it does not require the existence of distinct depositional periods (the existence of which has been questioned by Sanford & Halka 1993); it is also convenient mathematically since, as we shall see, it avoids singularities in the concentration field in very shallow water. (We shall in fact show that our results are robust to the value of ϵ which is employed.)

Equation (2.4), and equation (2.5) with $\epsilon = 0$, have been employed both in theoretical studies (e.g. Roberts *et al.* 2000; Pritchard & Hogg 2003) and in detailed numerical simulations of estuarine systems (e.g. Brenon & Le Hir 1999; Cancino & Neves 1999).

The sediment transport equation (2.3) can also be written in Lagrangian terms. We consider the concentration of sediment $\bar{c}_L(\hat{t})$ in a fluid 'parcel' with position $\hat{x}_L(\hat{t})$, depth $\hat{h}_L(\hat{t})$ and velocity $\mathrm{d}\hat{x}_L/\mathrm{d}\hat{t} = \bar{u}_L(\hat{t})$; equation (2.3) is then equivalent to

$$\frac{\mathrm{d}\bar{c}_L}{\mathrm{d}\hat{t}} = \frac{\hat{q}_e(\bar{u}_L) - \hat{q}_d(\bar{c}_L, \bar{u}_L)}{\hat{h}_L}. \tag{2.6}$$

2.1. *Non-dimensionalization*

Finally, we non-dimensionalize the governing equations, employing a horizontal length scale $\hat{L}_x$, a vertical length scale $\hat{L}_z = S\hat{L}_x$, a time scale $\hat{T}_0 = (\hat{L}_x/(S\hat{g}))^{1/2}$, a velocity scale $\hat{u}_0 = \hat{L}_x/\hat{T}_0 = (S\hat{g}\hat{L}_x)^{1/2}$ and a mass concentration scale $\hat{c}_0 = \hat{m}_e/\hat{w}_s$. Defining $h = \hat{h}/\hat{L}_z$, $x = \hat{x}/\hat{L}_x$, $u = \bar{u}/\hat{u}_0$ and $c = \bar{c}/\hat{c}_0$, we obtain the hydrodynamical equations

$$\frac{\partial h}{\partial t} + \frac{\partial}{\partial x}(uh) = 0, \quad \frac{\partial u}{\partial t} + u\frac{\partial u}{\partial x} = -\left(\frac{\partial h}{\partial x} + 1\right), \tag{2.7}$$

and the sediment transport equation

$$\frac{\partial c}{\partial t} + u\frac{\partial c}{\partial x} = E\left(\frac{q_e - q_d}{h}\right), \tag{2.8}$$

where

$$q_e = \begin{cases} \dfrac{u^2}{u_e^2} - 1 & \text{for } |u| \geqslant u_e, \\ 0 & \text{for } |u| < u_e, \end{cases} \tag{2.9}$$

and

$$q_d = \begin{cases} \epsilon c & \text{for } |u| > u_d, \\ c\left(1 - (1-\epsilon)\dfrac{u^2}{u_d^2}\right) & \text{for } |u| \leqslant u_d. \end{cases} \tag{2.10}$$

Here u_e and u_d are the dimensionless critical velocities for erosion and deposition, respectively, and $E = \hat{T}_0 \hat{w}_s / \hat{L}_z = \hat{w}_s / S(\hat{g}\hat{L}_z)^{1/2}$ represents the ratio of the settling velocity to the rate of vertical fluid motion.

2.1.1. *Reference values of parameters*

To illustrate our solutions, we consider as a reference case a rather steep flat of the kind associated with wave-dominated, erosional regimes (Kirby 1992), with gradient $S = 1/100$, and we consider long low-frequency waves with a period of the order of 150 s (so that if, as below, we define the period as $\hat{T} = \pi \hat{T}_0$ then $\hat{T}_0 \approx 50$ s). These values completely specify the hydrodynamic scales $\hat{L}_x = S\hat{g}\hat{T}_0^2 \approx 250$ m, $\hat{L}_z = S^2\hat{g}\hat{T}_0^2 \approx 2.5$ m, and $\hat{u}_0 \approx 5\ \mathrm{m\,s^{-1}}$. (These values are all rather large, but will be reduced somewhat as we consider waves under which the maximum velocity scales as $A\hat{u}_0$ for amplitudes A substantially less than 1.)

For muddy sediment, typical values of the settling velocity $\hat{w}_s$ are around $10^{-3}\ \mathrm{m\,s^{-1}}$, and typical values of the mass erosion rate $\hat{m}_e$ are around $5 \times 10^{-5}\ \mathrm{kg\,m^{-2}\,s^{-1}}$ (Roberts *et al.* 2000). The critical shear stress for erosion has been measured at between about 0.1 and $0.7\ \mathrm{N\,m^{-2}}$ which, using a quadratic drag law with coefficient $c_D = 0.003$ for a muddy bed (Dyer 1986), corresponds to critical velocities for erosion of between $0.18\ \mathrm{m\,s^{-1}}$ and $0.48\ \mathrm{m\,s^{-1}}$. As our main interest is in steep eroding flats on which the exposed sediment is typically well consolidated (see O'Brien *et al.* 2000 and references therein), we will consider values of $\hat{u}_e$ towards the upper end of this scale, and take $\hat{u}_e = 0.4\ \mathrm{m\,s^{-1}}$, and consequently $u_e = 0.08$. The bed exchange rate E therefore has the value $E = 0.02$. Finally, the quantity $\epsilon = \hat{w}_p / \hat{w}_s$ is rather hard to determine, owing to the complicated relationship between floc size, composition and settling velocity (Winterwerp 2002): we shall therefore take a reference value of $\epsilon = 0.05$ and consider other values ranging from $\epsilon = 0$ to $\epsilon = 1$. (We note that we have evaluated all the reference parameters only approximately, and we shall consider quite a broad range of variation about them.)

2.2. *Equilibrium concentrations and sediment fluxes*

It is useful for the subsequent discussion to define several quantities. The first is the instantaneous equilibrium concentration in a fluid parcel,

$$c_{eq}(t;\sigma_0) = \begin{cases} \dfrac{1}{\epsilon}\left(\dfrac{u^2}{u_e^2} - 1\right) & \text{when } |u| > u_e, \\ 0 & \text{when } |u| \leqslant u_e. \end{cases} \tag{2.11}$$

This represents an instantaneous balance between the erosion and deposition fluxes, and describes the concentration field in very shallow water where exchanges are very rapid. The second quantity is the long-term equilibrium concentration $c_T(\sigma_0)$ defined

such that

$$\int_0^T q_d(u_L(t;\sigma_0), c_T(\sigma_0))\,\mathrm{d}t = \int_0^T q_e(u_L(t;\sigma_0))\,\mathrm{d}t \tag{2.12}$$

for each fluid parcel. (Here σ_0 labels a Lagrangian fluid element and T is the period of the fluid motion.) This concentration corresponds to a balance between erosion and deposition over a period of the fluid motion: it describes the concentration field in deep water, where it changes only slowly throughout a period. Setting $c = c_T$ everywhere also provides a useful starting point for numerical integrations, as it reduces the time taken for the concentration field in deeper water to adjust to the periodic state: this initial condition was therefore used for all the results described here.

It is also useful to define two quantities which describe the sediment transport across the flat. The instantaneous Eulerian sediment flux $q(x, t)$ represents the total mass flux of suspended sediment passing a point x at time t, and is given by $q = cuh$. The time-integrated net flux Q then represents the total mass of sediment which passes this point in the course of one cycle, and is defined as $Q = \int_0^T q\,\mathrm{d}t$. The pattern of net transport $Q(x)$ is then the quantity most relevant to the long-term morphodynamics of the system. Both q and Q can readily be obtained numerically from the Lagrangian results by interpolation.

3. Hydrodynamics

3.1. *Carrier and Greenspan's wave solution*

Carrier & Greenspan (1958) demonstrated that by transforming to the independent variables

$$\lambda = 2(u + t), \quad \sigma = 4\sqrt{h}, \tag{3.1}$$

the shallow-water equations (2.1) and (2.2) may be rewritten as a single second-order linear equation,

$$\sigma\left(\frac{\partial^2 t}{\partial \lambda^2} - \frac{\partial^2 t}{\partial \sigma^2}\right) - 3\frac{\partial t}{\partial \sigma} = 0. \tag{3.2}$$

We now introduce a potential $\phi(\sigma, \lambda)$ such that

$$u = \frac{1}{\sigma}\frac{\partial \phi}{\partial \sigma}; \tag{3.3}$$

equation (3.2) is then equivalent to requiring that

$$\frac{\partial}{\partial \sigma}\left(\sigma\frac{\partial \phi}{\partial \sigma}\right) - \sigma\frac{\partial^2 \phi}{\partial \lambda^2} = 0, \tag{3.4}$$

and the remaining physical variables may be obtained as

$$x = \frac{1}{4}\frac{\partial \phi}{\partial \lambda} - \frac{\sigma^2}{16} - \frac{u^2}{2}, \quad h = \frac{\sigma^2}{16}, \quad t = \frac{\lambda}{2} - u. \tag{3.5}$$

The crucial feature of equation (3.4) is that it is linear, and it can be demonstrated (Carrier *et al.* 2003) that solutions can be expressed as the superposition of fundamental modes which correspond to cross-shore standing waves,

$$\phi_\omega(\sigma, \lambda) = A_\omega J_0(\omega\sigma)\cos(\omega\lambda - \psi), \tag{3.6}$$

where J_0 is the standard Bessel function, ω the angular frequency and ψ the relative phase of the wave. The transform (3.1) remains invertible (i.e. the wave does not

break) as long as the Jacobian $\partial(x,t)/\partial(\sigma,\lambda)$ never vanishes: for a monochromatic wave of angular frequency $\omega = 1$, this is equivalent to requiring that $|A_\omega| \leqslant 1$.

3.2. *Lagrangian formulation*

It is not possible in general to invert equations (3.5) explicitly to obtain $u(x,t)$ and $h(x,t)$, and it is therefore necessary to address the problem of tracking fluid parcels numerically. It would be possible in principle to do this by inverting the transformation numerically at each time step; however, computationally it is more accurate and efficient to view the advection in the transformed coordinates. We define $x_L = x(\sigma_L(t), \lambda_L(t))$, $u_L = u(\sigma_L(t), \lambda_L(t))$ and $h_L = h(\sigma_L(t), \lambda_L(t))$, where x, h and u are defined by equations (3.3) and (3.5), and t parameterizes the particle path. The parcel advection equation $\mathrm{d}x_L/\mathrm{d}t = u_L$ now yields

$$\frac{\mathrm{d}\sigma_L}{\mathrm{d}t}\left[\frac{1}{4}\frac{\partial^2\phi}{\partial\sigma\,\partial\lambda} - \frac{1}{8}\sigma_L + \frac{1}{\sigma_L^3}\left(\frac{\partial\phi}{\partial\sigma}\right)^2 - \frac{1}{\sigma_L^2}\left(\frac{\partial\phi}{\partial\sigma}\right)\frac{\partial^2\phi}{\partial\sigma^2}\right] + \frac{\mathrm{d}\lambda_L}{\mathrm{d}t}\left[\frac{1}{4}\frac{\partial^2\phi}{\partial\lambda^2} - \frac{1}{\sigma_L^2}\left(\frac{\partial\phi}{\partial\sigma}\right)\frac{\partial^2\phi}{\partial\sigma\,\partial\lambda}\right] = \frac{1}{\sigma_L}\frac{\partial\phi}{\partial\sigma}, \quad (3.7)$$

where the derivatives of ϕ are understood to be evaluated at (σ_L, λ_L).

Requiring that the parametric variable t corresponds to the time variable $t_L = t(\sigma_L, \lambda_L)$ measured along the particle path then yields a second equation, $\mathrm{d}t_L/\mathrm{d}t = 1$, and thus

$$\frac{\mathrm{d}\sigma_L}{\mathrm{d}t}\left[\frac{1}{\sigma_L^2}\frac{\partial\phi}{\partial\sigma} - \frac{1}{\sigma_L}\frac{\partial^2\phi}{\partial\sigma^2}\right] + \frac{\mathrm{d}\lambda_L}{\mathrm{d}t}\left[\frac{1}{2} - \frac{1}{\sigma_L^2}\frac{\partial^2\phi}{\partial\sigma\,\partial\lambda}\right] = 1. \quad (3.8)$$

Although they are strongly nonlinear in σ_L and λ_L, these equations may easily be integrated forwards in time, together with the associated concentration equation

$$\frac{\mathrm{d}c_L}{\mathrm{d}t} = \frac{16E}{\sigma_L^2}\left[q_e(u(\sigma_L, \lambda_L)) - q_d(c_L, u(\sigma_L, \lambda_L))\right]. \quad (3.9)$$

This was implemented employing a standard fourth-order Runge–Kutta routine together with series representations for the Bessel functions, both taken from Press *et al.* (1992).

It is simple to obtain information about the concentration, velocity and depth fields either in Lagrangian form, following a particular fluid parcel, or as 'snapshots' at a particular point in time, parameterized by a parcel labelling parameter such as the initial value $\sigma_0 = \sigma_L(t_0)$. (Note that in the case of a monochromatic wave with $\psi = 0$, it is convenient to take $t_0 = \pi/4$, so $u(x, t_0) = 0$ everywhere, and $\lambda_0 = \pi/2$.)

4. Sediment transport under a monochromatic wave

We now present the results of a series of numerical integrations of the system described above, for a variety of values of the governing parameters. It was found that, regardless of the initial condition for the suspended sediment in each fluid parcel, the concentration field adjusted over a few cycles to a periodic state, and it is this which we discuss from this point onwards.

Our reference case in this section is a standing wave with dimensionless amplitude $A = 0.2$ and frequency $\omega = 1$ so that the dimensionless maximum velocity under the wave is $u = A/2 = 0.1$, and we employ the parameter values described in § 2.1.1. We start by describing this case in some detail, and then consider the effect of varying the parameters.

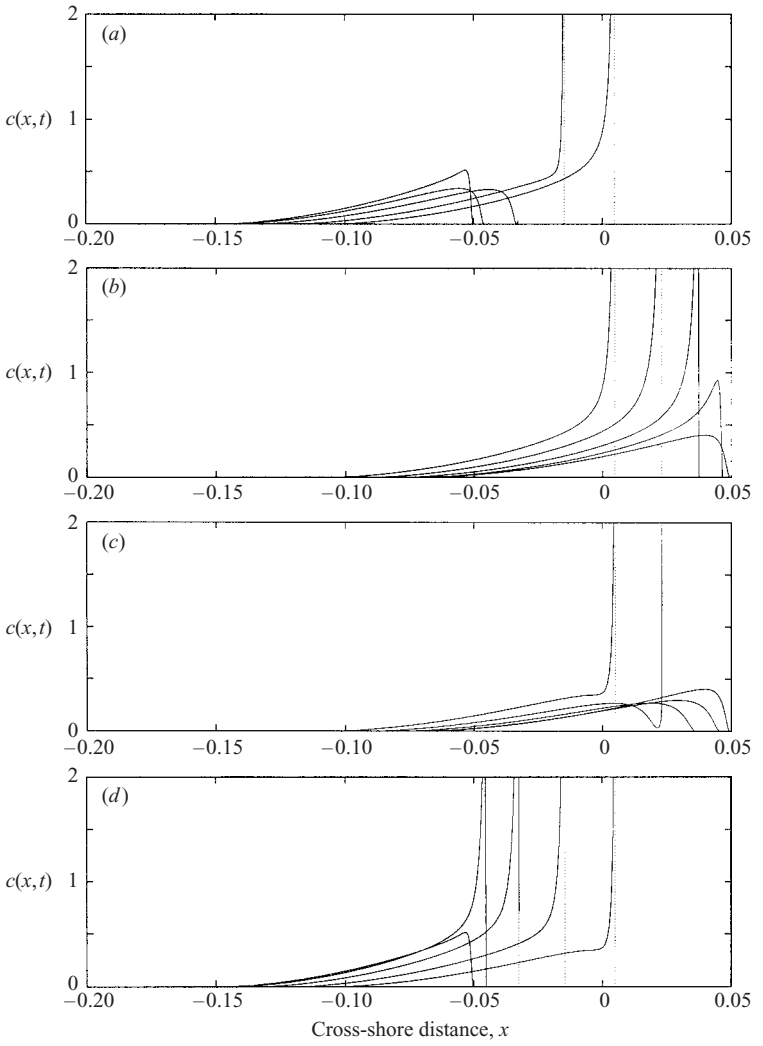

FIGURE 2. Periodic solution for suspended sediment concentration on a linear beach, under Carrier–Greenspan flow with $A = 0.2$, $E = 0.02$, $u_e = 0.08$, $u_d = 0.056$ and $\epsilon = 0.05$: plots at intervals of $\pi/16$. (*a*) first half of run-up; (*b*) second half of run-up; (*c*) first half of run-down; (*d*) second half of run-down. The c-axis has been truncated at $c = 2$ for visual convenience, although in very shallow water the maximum value of c is approximately $c = 11$ (see equation (2.11) and figure 3).

4.1. *Reference case*

Our reference solution is illustrated in figures 2, 3 and 4. Figure 2 shows the concentration field in Eulerian form, figure 3 shows the concentration and velocity fields in Lagrangian form, and figure 4 shows the Eulerian quantities $q(x, t)$ and $Q(x)$.

4.1.1. *Concentration field*

The first noticeable feature of figure 2 is that the concentration field is spatially localized. The first zero in the velocity of the standing wave defined by equation (3.6) occurs at the first zero of the Bessel function J_1, in other words at $\sigma = \sigma_1 \approx 3.83$ (Abramowitz & Stegun 1965), where the undisturbed water depth is around $h = 0.92$.

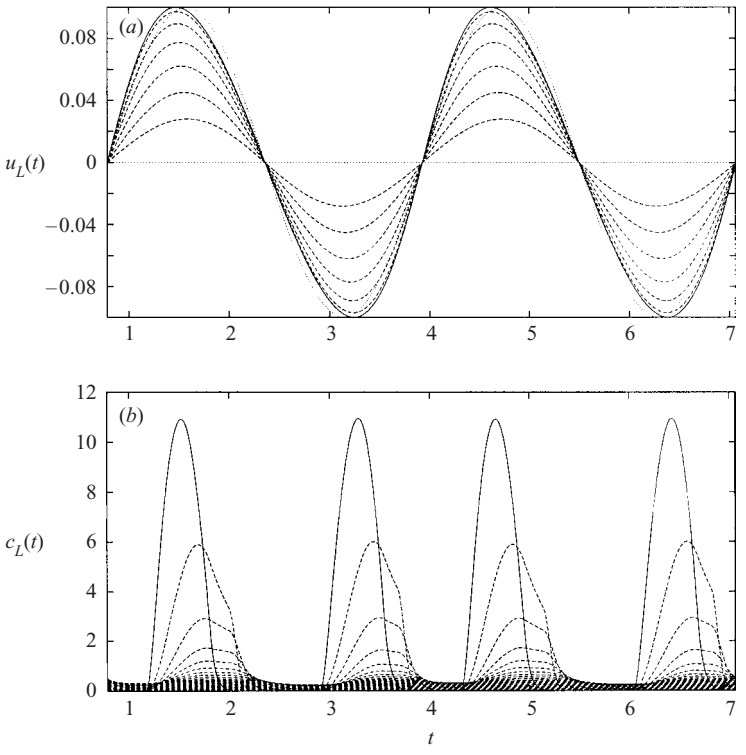

FIGURE 3. Periodic solution over two periods ($t = \pi/4$ to $9\pi/4$) with $A = 0.2$, $E = 0.02$, $\epsilon = 0.05$, $u_e = 0.08$, $u_d = 0.056$: (*a*) Lagrangian velocity $u_L(t)$ and (*b*) Lagrangian concentration $c_L(t)$. In each case the shoremost fluid parcel (solid line) is at $\sigma_0 = 0.03$; dashed lines represent fluid parcels behind the shoreline. In (*a*) the dotted lines represent $u = 0.1 \sin(2t - \pi/2)$ and $u = 0$.

In this region, the velocity is insufficient ever to mobilize sediment. However, the localization of the concentration field is considerably stronger than this would suggest, and is due more to the rapid decay of the 'envelope' of the Bessel function, which means that it is only in the nearshore region that velocities are high enough to suspend sediment.

The other prominent feature of figure 2 is the pronounced peak in concentration near the shoreline (the *turbid fluid edge*), which forms during erosional periods. (The concentration at the shoreline is bounded by c_{eq}; however, the c-axis in figure 2 has been truncated to make the details of the concentration field elsewhere more apparent.) This feature occurs essentially because in the shallow water near the shoreline the entrainment of sediment produces rather high concentrations, which are strongly correlated with the local velocity. The turbid edge is readily observed in the field (see, for example, Christie & Dyer 1998), and its behaviour is also the clearest illustration in the Eulerian frame of the mechanisms called settling lag and scour lag, which play an important part in redistributing sediment across the flat.

Settling and scour lag are most easily visualized when the solution is displayed in Lagrangian form (figure 3). They consist of the delayed response of the concentration field to changes in the velocity, which is caused by the finite time which it takes sediment to settle out of suspension (settling lag) and the finite time taken to erode sediment once velocities have increased above u_e (scour lag). (These delays should not be confused with the 'response time' associated with the vertical distribution

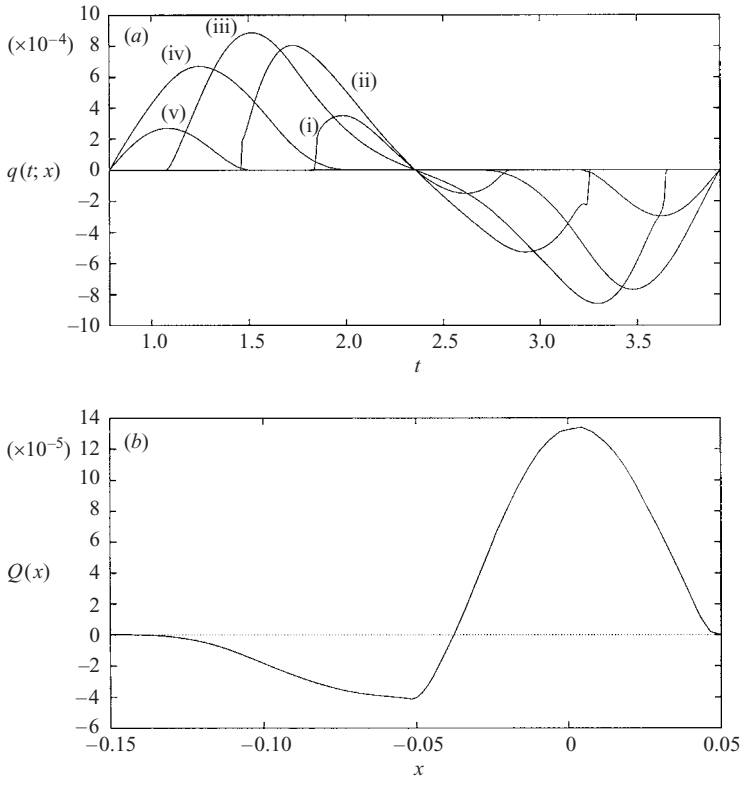

FIGURE 4. Landwards flux of sediment under Carrier–Greenspan flow, for $A = 0.2$, $E = 0.02$, $u_e = 0.08$, $u_d = 0.056$ and $\epsilon = 0.05$. (*a*) Instantaneous fluxes $q(t; x)$ over a period ($t = \pi/4$ to $5\pi/4$), measured at: (i) $x = 0.0325$; (ii) $x = -0.0025$; (iii) $x = -0.0375$; (iv) $x = -0.0725$; (v) $x = -0.1075$. (*b*) Net flux $Q(x)$ over a period.

of sediment in the water column (Stansby & Awang 1998), although this may be expected to accentuate lag effects.)

The processes by which lag effects lead to net sediment transport have been discussed in detail elsewhere (Nichols & Biggs 1985; Pritchard & Hogg 2003). The essential mechanism is that the finite response time in the Lagrangian frame translates into a phase lag in the Eulerian frame between the concentration and velocity fields; consequently, the Eulerian sediment fluxes $q(x, t)$ are different on the run-up and run-down, and do not necessarily cancel out when integrated over a tidal cycle. Settling lag has been postulated in several coastal situations as a principal mechanism by which a tidal flow can lead to net sediment transport, and it is generally believed to favour the landwards transport of sediment, especially in the inland reaches of estuaries or tidal inlets.

Settling and scour lag are most readily apparent in fluid parcels a little way behind the shoreline, where the quantity E/h_L is of order 1; in other words, where the water is sufficiently deep that sediment takes a noticeable time to settle out of suspension, but is not so deep that the concentrations change little over the course of a hydrodynamic period, and consequently remain close to c_T throughout. We may therefore expect settling and scour lag to have most effect on the net transport in this region.

The other point which these plots illustrate is the asymmetry of the hydrodynamics experienced by a fluid parcel. This is made clearest in figure 3(*a*), where $u_L(t)$ for

several fluid parcels is compared with a sinusoidal curve: it is clear that the period when velocities are decreasing is longer than the period when they are increasing, and so fluid accelerations are greater around $t = \pi/4$ (maximum run-down) than around $t = 3\pi/4$ (maximum run-up). This explains why the turbid edge is more pronounced at the end of run-down than at the end of run-up (figure 2), as more material has time to settle out during the purely depositional period around $t = 3\pi/4$: we may expect this also to lead to the net movement of sediment up the flat.

The combination of lag effects and greater deposition around maximum run-up may be expected to lead to shorewards net sediment transport, at least on the upper part of the flat, and we now consider the sediment fluxes in more detail to confirm that this is the case.

4.1.2. *Sediment fluxes*

Figure 4 illustrates the instantaneous and net cross-shore sediment fluxes $q(x, t)$ and $Q(x)$.

The maximal instantaneous seaward and landward fluxes are both low on the uppermost part of the inundated region, as fluid depths and thus total sediment loads here are always low. They increase towards a maximum in the region of $x = -0.03$, which is affected by the high concentrations in the body of the flow behind the turbid edge, and they then decrease seawards along with sediment concentrations.

The signature of the turbid fluid edge itself is also evident in figure 4(a). Despite the dominance of this feature in figure 2, it occurs only in very shallow water, and so it shows up in the flux data only as a small kink in q very close to the start and end of inundation. This suggests that, while the turbid fluid edge is a prominent feature of our solutions, the accurate representation and measurement of concentrations in this region is not of great significance for the prediction of net sediment transport, because both the lag effects and the total sediment load are small in this region – we return to this point in the next section.

The pattern of net sediment flux $Q(x)$ is shown in figure 4(b). In the upper part of the active region, corresponding roughly to the swash zone, there is a net shorewards movement of sediment, with deposition above about $x = 0.005$ and erosion below. (It is also notable that the peak value of the net fluxes in this region is a significant fraction of the peak value of the instantaneous fluxes, indicating the strong asymmetry between run-up and run-down sediment transport in this region.) This landwards transport may be attributed to settling lag, with material being eroded on the run-up and deposited around $t = 3\pi/4$.

In the lower part of the active region, the direction of net flux reverses, with material being eroded from around the point of minimum shoreline penetration and deposited further seawards. This offshore flux gradually decays seawards until it reaches the low-velocity region where there is no sediment mobilization and consequently no net transport.

This net seawards movement of sediment is a feature which is not found under cross-shore tidal currents (Pritchard & Hogg 2003). It occurs because of the lower concentrations which occur towards the velocity node of the standing wave: on the run-up, these low concentrations are advected landwards, so that even though sediment is being eroded, the peak of q on the run-up is slightly lower than that on the run-down in this region of the flat. (Compare the positive and negative peaks of q for line (iv) in figure 4a.) This effect is rather weak, and in the upper part of the active region it is easily swamped by the shoreward transport due to settling lag, but

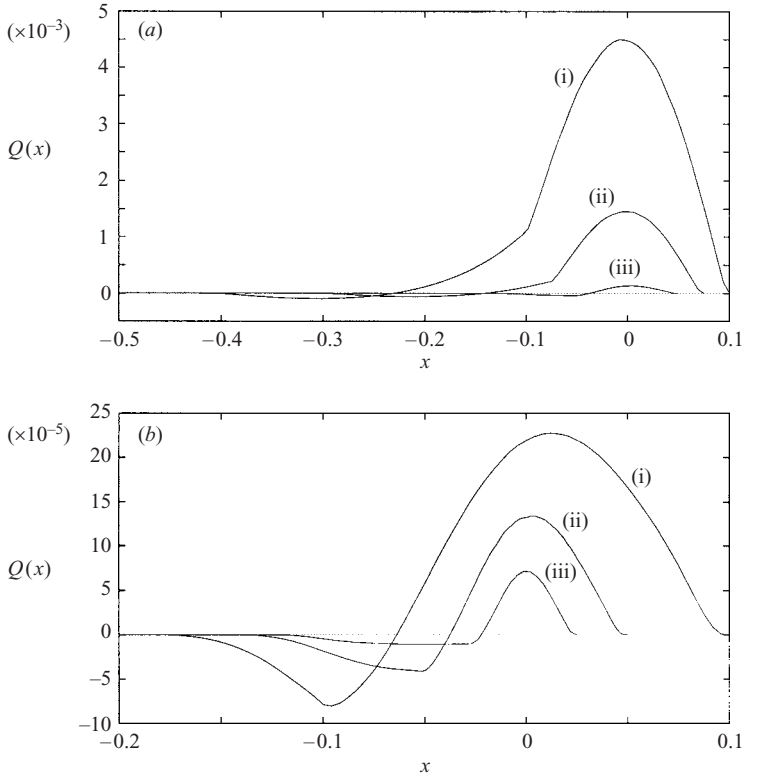

FIGURE 5. Net landwards flux of sediment, for $E = 0.02$, $\epsilon = 0.05$ and: (*a*) $u_e = 0.08$, $u_d = 0.056$ and: (i) $A = 0.4$; (ii) $A = 0.3$; (iii) $A = 0.2$; (*b*) (i) $A = 0.4$, $u_e = 0.16$, $u_d = 0.112$; (ii) $A = 0.2$, $u_e = 0.08$, $u_d = 0.056$; (iii) $A = 0.1$, $u_e = 0.04$, $u_d = 0.028$.

in deeper regions, where Lagrangian concentrations vary less over a cycle and so lag effects are reduced, it makes its presence felt.

4.2. *Varying physical parameters*

We have also carried out a series of numerical integrations to investigate the effects on the concentration field and the net fluxes of varying the physical parameters A, E, ϵ, u_e and u_d. We restrict ourselves here to a brief description of the most important results.

When the amplitude A is increased keeping all other parameters constant, the effect is predictably to increase the region in which sediment is mobilized, as well as to cause substantially higher concentrations. Because of the higher fluid accelerations, lag effects are enhanced, and so the landwards net transport is enhanced relative to the seawards net transport; the overall features of $Q(x)$, however, remain the same (figure 5*a*). By contrast, when A is increased or reduced and the critical velocities u_e and u_d are increased or reduced in proportion (so that it is merely the relative nonlinearity of the standing wave hydrodynamics which are altered), the increase is much less pronounced (figure 5*b*), and the region of net seaward flux is the more enhanced; the dividing line between positive and negative Q, however, also moves seawards as lag effects in the landward region are enhanced by the greater accelerations.

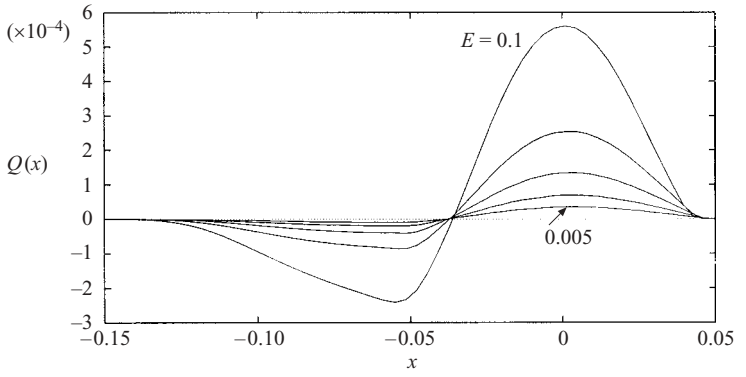

FIGURE 6. Net landward flux of sediment, for $A = 0.2$, $\epsilon = 0.05$, $u_e = 0.08$, $u_d = 0.056$ and $E = 0.1$, 0.04, 0.02, 0.01 and 0.005.

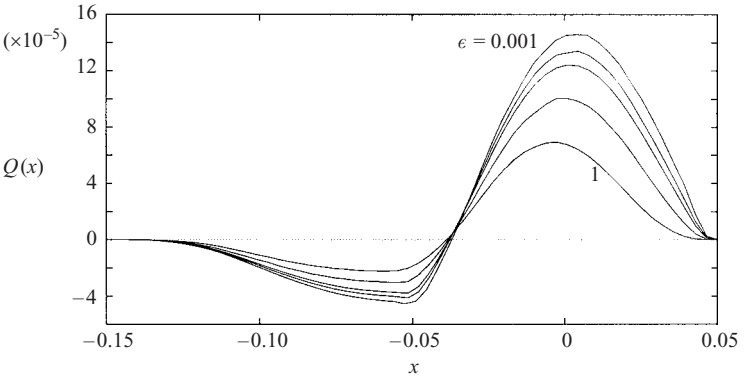

FIGURE 7. Net landward flux of sediment, for $A = 0.2$, $E = 0.02$, $u_e = 0.08$, $u_d = 0.056$ and $\epsilon = 0.001$, 0.05, 0.1, 0.3 and 1.0. (The case $\epsilon = 0$ is omitted as it is difficult to obtain numerical stability in shallow water in this case.)

The effect of varying the bed exchange rate E is illustrated in figure 6. As E increases, more sediment can be deposited during phases of low u, and so the net sediment transport is enhanced. However, the pattern remains the same as before.

Both c and Q vary as might be expected with the critical velocity for erosion u_e: lower values of u_e increase concentrations, especially near the shoreline, and thus increase net landwards transport, while increasing u_e eventually leads to a situation in which no sediment is mobilized at all. The critical velocity for deposition u_d, on the other hand, appears to exert only a very slight influence on Q, since a substantial proportion of the net deposition takes place through the settling of primary particles when $u > u_d$.

Finally, we consider the control which the heuristic parameter ϵ exerts on our results (figure 7). Reducing ϵ has a dramatic effect on plots of $c(x, t)$, because of the effect it has on c_{eq} and thus on the turbid fluid edge. However, its effect on the magnitude of the net fluxes is less pronounced, in agreement with our previous observation that the turbid edge has only a small signature in plots of the instantaneous flux q. In addition, the pattern of net flux is qualitatively unaltered even when ϵ is increased to its limiting value of 1. This suggests that our results do not depend strongly on the details of the depositional model which we have chosen to employ.

5. Combining different modes of oscillation

While the standing wave described in the preceding section illustrates the basic role of settling lag under infragravity waves, it can be misleading to consider the effects of infragravity motion in terms of a single standing wave with a well-defined frequency and cross-shore wavelength. The spectra of wave energy observed on natural beaches typically show a range of frequencies in the infragravity band rather than a sharply defined peak, and this may have significant consequences for sediment transport patterns. In particular, Holman & Sallenger (1993) considered the hypothesis that a node in the cross-shore velocity might provide a mechanism for bar generation on sandy beaches, and demonstrated that this theory was not supported by field data in the presence of a wider spectrum of infragravity waves.

Our interest in this study, as indicated, is not in transport near the nodes of the standing wave, but in the swash zone of the flat, where the majority of the net sediment flux occurs. However, it is important to investigate the effect on the sediment transport of combining several frequencies of infragravity oscillation.

As noted in § 3, the linearity of the transformed governing equation (3.4) allows us to superimpose any number of solutions of the form (3.6); given such a compound solution, the governing equations (3.7), (3.8) and (3.9) may be formulated and integrated as before.

In this section, we will consider the effect of combining only two modes. This is clearly a considerable simplification of the hydrodynamics. However, it provides a basis for the study of more complete spectra by elucidating some features of transport under interacting modes, and the periodicity of the hydrodynamics makes interpretation of the results somewhat clearer than under a more complex spectrum.

The bimodal oscillation has the form

$$\phi(\sigma, \lambda) = A_1[(1-\beta)J_0(\sigma)\cos\lambda + \beta J_0(\omega\sigma)\cos(\omega\lambda - \psi)], \tag{5.1}$$

where $0 \leqslant \beta < 1$, and where A_1 is a modified amplitude and ψ a relative phase for the bimodal oscillation. We recover the monotonic wave of the previous section either by setting $\beta = 0$ or by setting $\omega = 1$ and $\psi = 0$ simultaneously.

The modified amplitude A_1 is chosen in order to make the compound oscillation comparable to the simple standing wave. From the point of view of energetics, it is natural to normalize some quantity proportional to u^2; as this is also the key quantity in the entrainment and deposition of sediment, we will adopt this approach, and choose A_1 such that the quantity

$$\left(\frac{A_0}{4}\right)^2 \equiv \frac{1}{T_\omega}\int_0^{T_\omega} u_{sh}^2(t)\,\mathrm{d}t \tag{5.2}$$

is a constant, where u_{sh} is the velocity at the shoreline, and where T_ω is the period of the compound oscillation. (For simplicity, we consider here only rational values $\omega = m/n$ for $m, n \in \mathbb{N}$: the period is then given by $T_\omega = 2\pi n$.) A_0^2 may be rewritten as

$$A_0^2 = \frac{16}{\Lambda_\omega}\int_0^{\Lambda_\omega}\left(\frac{1}{\sigma}\frac{\partial\phi}{\partial\sigma}\right)^2_{|\sigma=0}\left(\frac{1}{2} - \frac{1}{\sigma}\frac{\partial^2\phi}{\partial\lambda\partial\sigma}\right)_{|\sigma=0}\mathrm{d}\lambda, \tag{5.3}$$

where $\Lambda_\omega = 2T_\omega$, and it is straightforward to obtain the result

$$A_0^2 = \begin{cases} A_1^2[(1-\beta)^2 + \beta^2\omega^4] & \text{when } \beta > 0,\ \omega \neq 1, \\ A_1^2 & \text{when } \beta = 0,\ \omega = 1, \end{cases} \tag{5.4}$$

for the bimodal oscillation (5.1).

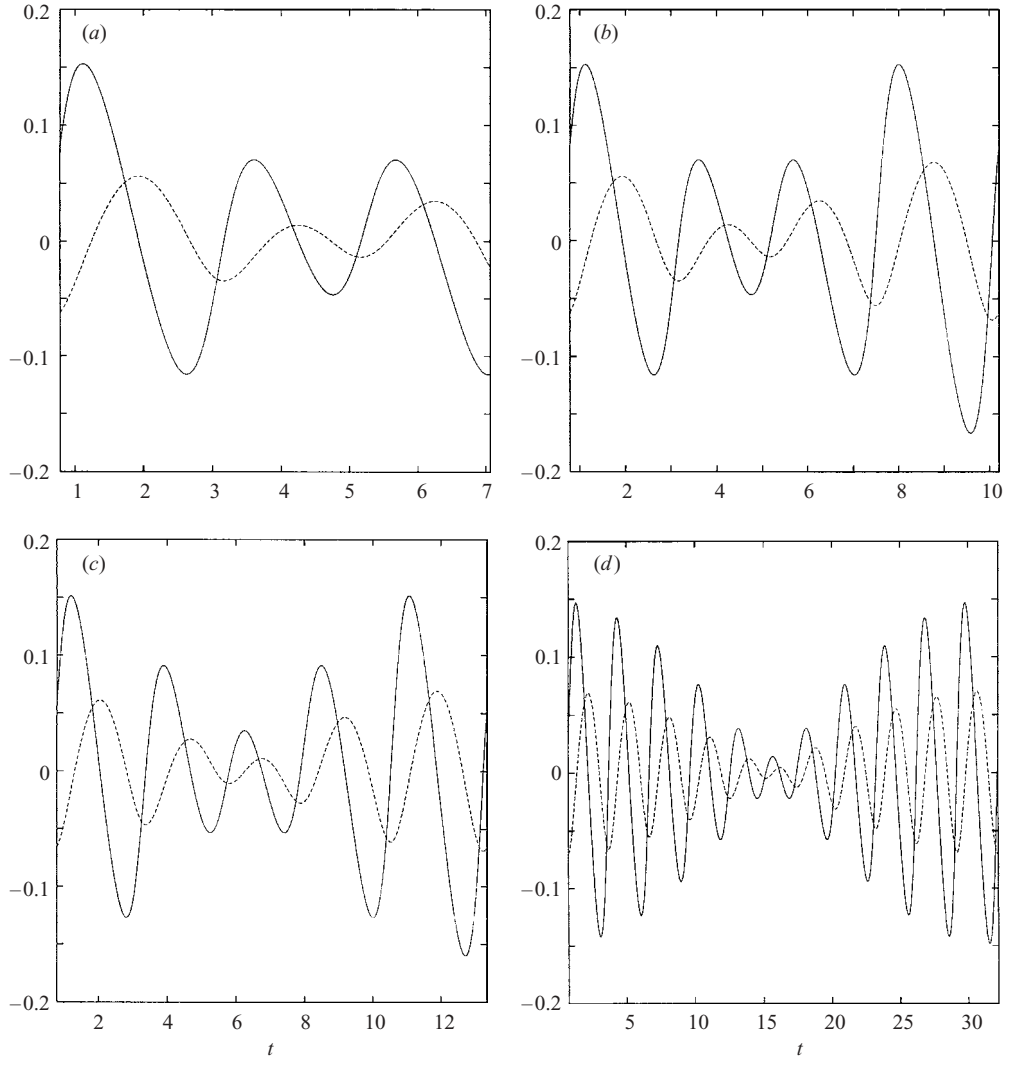

FIGURE 8. Position (dashed line) and velocity (solid line) of the shoreline fluid parcel under bimodal oscillatory flow with $\beta = 1/2$ and $\psi = 0$. (*a*) $\omega = 3/2$ ($A_1 = 0.22188$); (*b*) $\omega = 4/3$ ($A_1 = 0.24000$); (*c*) $\omega = 5/4$ ($A_1 = 0.24988$); (*d*) $\omega = 11/10$ ($A_1 = 0.26907$).

We will consider variations in two of the parameters which describe the compound oscillation: the secondary frequency ω and the relative phase ψ. To represent a strong interaction, we take $\beta = 1/2$ throughout.

5.1. *Varying the secondary frequency* ω

We consider values of ω fairly close to the basic frequency 1, as we are interested primarily in the interaction of nearby modes within the infragravity band.

Figure 8 illustrates the near-shore hydrodynamics in Lagrangian form for the four cases $\omega = 3/2$, $\omega = 4/3$, $\omega = 5/4$ and $\omega = 11/10$. As ω approaches 1, the variation in the nearshore velocities increases, with higher peak velocities but also longer periods of low velocity; when ω is quite close to 1, a strong beat effect is evident. The range

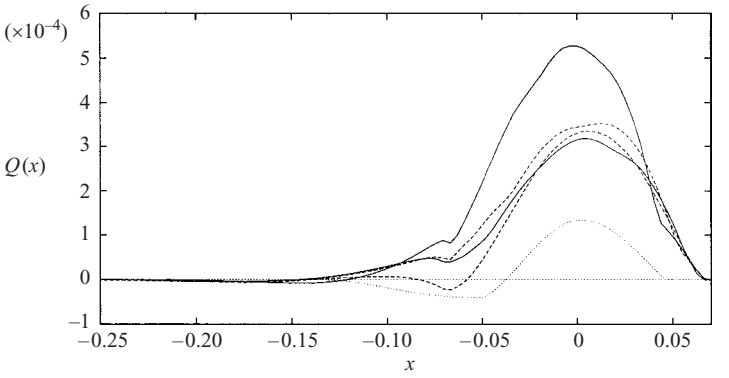

FIGURE 9. Net landwards flux of sediment under bimodal oscillations, for $E = 0.02$, $u_e = 0.08$, $u_d = 0.056$, $\epsilon = 0.05$, and: $\omega = 3/2$ (upper solid line); $\omega = 4/3$ (upper dashed line); $\omega = 5/4$ (lower solid line); $\omega = 11/10$ (lower dashed line). The reference case $\beta = 0$ is also shown (dotted line).

of the swash remains roughly constant, with the maximum run-up position between $x = 0.06$ and $x = 0.07$ and the maximum run-down between $x = -0.06$ and $x = -0.07$.

Figure 9 shows the corresponding net fluxes of sediment across the flat. As under the monochromatic standing wave, the fluxes are strongly localized within the swash zone, but two differences are evident from the simpler case. The first is the generally higher fluxes, which occur because the peak velocities which dominate sediment transport are higher under the bimodal wave; to some extent this feature is a consequence of the normalization chosen for A_1. The second feature is that landwards transport in the swash zone and just offshore is substantially enhanced compared to the seawards transport which was evident for the monochromatic wave. This occurs because there is no longer a node of the velocity field in this region, and so the ability of the low-velocity region to trap sediment through settling lag is much reduced.

As ω is reduced, the pattern of net transport becomes closer in form to the monochromatic case, and the maximum of $Q(x)$ reduces slightly. As under the monochromatic wave, the position of maximum run-down is associated with a change in the gradient $\partial Q/\partial x$, and thus with quite a rapid change in the net erosion. This illustrates the important role of the region just behind the shoreline in mobilizing sediment in the swash zone, remarked on by Christie & Dyer (1998).

5.2. *Varying the relative phase* ψ

Figure 10 illustrates the effect on the hydrodynamics of varying the relative phase ψ for the case $\omega = 3/2$, while figure 11 shows the net sediment fluxes for each case.

As can be seen from figure 10, altering the relative phase ψ has two effects: first, it alters the sequence of strong and weak uprush and backwash events; and second, it introduces a slight asymmetry in the hydrodynamics, with peak velocities being either in the seawards or in the landwards direction. (This is most evident when the lines for $\psi = 0$ and $\psi = \pi/2$ are compared with $u = \pm 0.15$, which is plotted for visual convenience.)

Since sediment transport is dominated by the peak velocities attained by the flow, the asymmetry in peak velocities might be expected to influence the net flux of sediment. The strength of the asymmetry may be gauged by calculating the maximum value of the erosion rate q_e: for $\psi = 0$ the maximum erosion rate is 44% higher during flow in the seawards direction than during flow in the landwards direction,

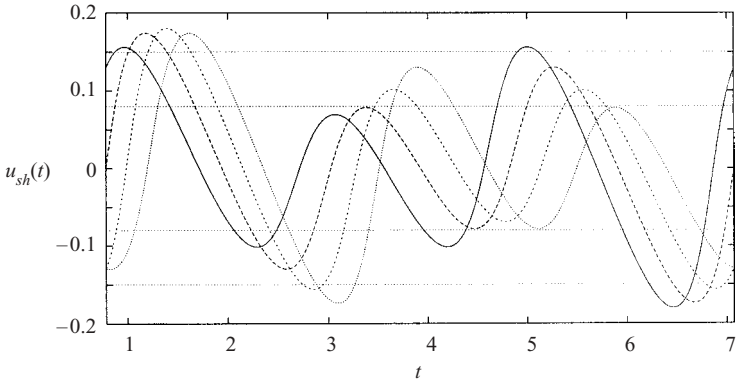

FIGURE 10. Shoreline velocity $u_{sh}(t)$ under bimodal oscillations, for $E=0.02$, $u_e=0.08$, $u_d=0.056$, $\epsilon=0.05$, $\omega=3/2$ and: $\psi=0$ (solid line); $\psi=\pi/4$ (heavy dashed line); $\psi=\pi/2$ (light dashed line); $\psi=3\pi/4$ (dotted line). The horizontal dotted lines represent $u=\pm0.15$ and $u=\pm0.08$.

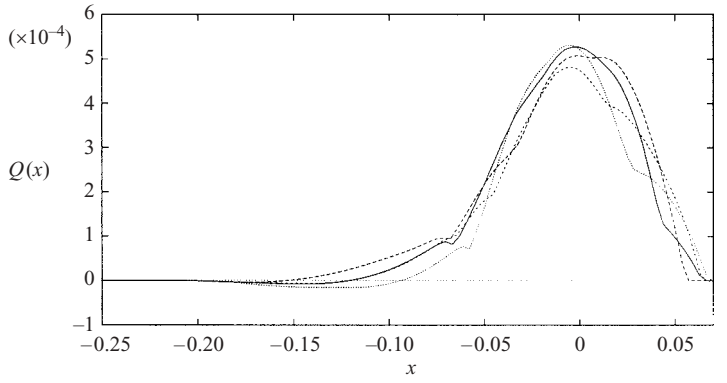

FIGURE 11. Net landwards flux of sediment under bimodal oscillations, for $E=0.02$, $u_e=0.08$, $u_d=0.056$, $\epsilon=0.05$, $\omega=3/2$ and: $\psi=0$ (solid line); $\psi=\pi/4$ (heavy dashed line); $\psi=\pi/2$ (light dashed line); $\psi=3\pi/4$ (dotted line).

while for $\psi=\pi/2$ the situation is reversed. Figure 11, however, shows that the net sediment transport is only very weakly influenced by this: the fluxes for $\psi=0$ and $\psi=\pi/2$ are comparable in the swash zone, and almost identical further offshore.

The more substantial difference is between the net fluxes for $\psi=\pi/4$ and $\psi=3\pi/4$: the former is biased more strongly in favour of landward transport even though they have identical maximum and minimum velocities. An explanation can be found in the sequence in which on- and offshore peak flows occur. The onshore peak in velocity for $\psi=\pi/4$ is followed by a weaker offshore flow and then by a period of low onshore velocities, allowing the sediment mobilized around $t=1$ to be carried landwards. The onshore peak in velocity for $\psi=3\pi/4$, on the other hand, is succeeded by a strong offshore flow, reducing the tendency of settling lag to move material landwards.

Overall, however, the most striking feature of figure 11 is that the general pattern of transport across the swash zone is very similar in each case, further indicating the robustness of this pattern to the details of the hydrodynamics on the flat.

6. Conclusions and applications

We have presented solutions for the erosion, deposition and suspended transport of fine sediment in and just beyond the swash zone under 'leaky' infragravity waves reflected from a linear beach or flat. The concentration field adjusts rapidly to a periodic state, in which settling lag effects lead to a pronounced landward movement of sediment across the swash zone. This pattern of landward transport is robust to a wide range of variation in the physical parameters, and it occurs under both monochromatic waves and more complicated wave patterns, including some for which the peak velocities are directed seawards.

For some forms of oscillation, in particular monochromatic waves and those where the dominant frequencies are close together, there is also a small seaward flux further offshore, so that sediment is preferentially eroded from the lower part of the swash zone and deposited further up or down the beach. This feature is associated with the presence of a region of rather low velocities not far offshore, and is therefore likely to occur only where a well-defined cross-shore standing wave occurs, for example as the result of a resonance between wave forcing and the local estuarine bathymetry.

A final important finding is that the net pattern of sediment transport may be affected less by the direction of peak velocities than by the sequence in which peak on- and off-shore flows occur. This is a factor which should be taken into account in future efforts to develop parameterized time-integrated descriptions of swash zone sediment transport.

Our findings suggest that advection by infragravity waves does not contribute to the tendency of wave-dominated hydrodynamics to export sediment from a muddy shore. However, it may be significant in redistributing sediment within the nearshore region and the swash zone.

The parameters employed in this study to describe sediment entrainment and deposition are appropriate for fine cohesive sediment. However, the model described is applicable to more general classes of material. In particular, it would be relatively straightfoward to repeat these calculations with parameters which were suitable to describe the behaviour of coarser cohesionless particles such as fine sand, and thus to obtain further insight into the dynamics of sandy beaches under infragravity waves. (We note that the robustness of our results to the details of the erosion and deposition models suggest that the pattern of transport is likely to be similar for the different sediment types.)

The method presented here for investigating sediment transport within the formalism due to Carrier & Greenspan (1958) has the advantage that it easily resolves and tracks the position of the shoreline and the sediment dynamics in this region, including a realistic turbid fluid edge. This is in contrast to the severe problems encountered in many numerical investigations, and the simplicity of their construction may make these solutions suitable as a test case for such investigations, complementary to the well-established test solutions for the hydrodynamics.

Various extensions of the present study could also be accomplished within the framework described here. In particular, it would be natural to consider sediment transport under more complex hydrodynamics; for example, the solutions discussed by Carrier *et al.* (2003) and others; or stochastic forcing reflecting the 'white noise' character of many measured infragravity spectra. The absence of a well-defined period for the fluid motion would constitute an extra complication in the interpretation of transport patterns, and is a principal reason why these problems lie beyond the scope of the current paper. However, such investigations would provide insight into an important question in this area of research, which is to assess the long-term sediment

transport associated with wind-generated waves across an intertidal flat, with the aim of clarifying their morphodynamic role.

D. P. and A. J. H. acknowledge the financial support of EPSRC; D. P. also acknowledges the financial support of the BP Institute. We would like to thank several anonymous reviewers for their constructive comments and for bringing aspects of the existing literature to our attention.

REFERENCES

Abramowitz, M. & Stegun, I. A. 1965 *Handbook of Mathematical Functions.* Dover.

Baldock, T. E. & Holmes, P. 1999 Simulation and prediction of swash oscillations on a steep beach. *Coastal Engng* **36**, 219–242.

Barnes, T. 1996 The generation of low-frequency water waves on beaches. PhD thesis, University of Bristol.

Bass, S. J., Aldridge, J. N., McCave, I. N. & Vincent, C. E. 2002 Phase relationships between fine sediment suspensions and tidal currents in coastal seas. *J. Geophys. Res.* **107**(C10), 3146.

Brenon, I. & Le Hir, P. 1999 Modelling the turbidity maximum in the Seine estuary (France). *Est. Coast. Shelf Sci.* **49**, 525–544.

Cancino, L. & Neves, R. 1999 Hydrodynamic and sediment suspension modelling in estuarine systems. *J. Mar. Sys.* **22**, 105–116.

Carrier, G. F. & Greenspan, H. P. 1958 Water waves of finite amplitude on a sloping beach. *J. Fluid Mech.* **4**, 97–109.

Carrier, G. F., Wu, T. T. & Yeh, H. 2003 Tsunami run-up and draw-down on a plane beach. *J. Fluid Mech.* **475**, 79–99.

Christie, M. C. & Dyer, K. R. 1998 Measurements of the turbid tidal edge over the Skeffling mudflats. In *Sedimentary Processes in the Intertidal Zone* (ed. K. S. Black, D. M. Paterson & A. Cramp). Geological Society, London.

Christie, M. C., Dyer, K. R. & Turner, P. 1999 Sediment flux and bed level measurements from a macro-tidal mudflat. *Est. Coast. Shelf Sci.* **49**, 667–688.

Dyer, K. R. 1986 *Coastal and Estuarine Sediment Dynamics.* Wiley.

Dyer, K. R. 1998 The typology of intertidal mudflats. In *Sedimentary Processes in the Intertidal Zone* (ed. K. S. Black, D. M. Paterson & A. Cramp). Geological Society, London.

Dyer, K. R., Christie, M. C., Feates, N., Fennessy, M. J., Pejrup, M. & van der Lee, W. 2000 An investigation into processes influencing the morphodynamics of an intertidal mudflat, the Dollard estuary, The Netherlands. *Est. Coast. Shelf Sci.* **50**, 607–625.

Dyer, K. R. & Soulsby, R. L. 1988 Sand transport on the continental shelf. *Annu. Rev. Fluid Mech.* **20**, 295–324.

Einstein, H. A. & Krone, R. B. 1962 Experiments to determine modes of cohesive sediment transport in salt water. *J. Geophys. Res.* **67**, 1451–1461.

Flemming, B. W. 2002 Geographic distribution of muddy coasts. In *Muddy Coasts of the World* (ed. T. Healy, Y. Wang & J.-A. Healy). Elsevier.

Friedrichs, C. T. & Aubrey, D. G. 1996 Uniform bottom shear stress and equilibrium hypsometry of intertidal flats. In *Mixing in Estuaries and Coastal Seas* (ed. C. Pattiaratchi). American Geophysical Union.

Hibberd, S. & Peregrine, D. H. 1979 Surf and run-up on a beach: a uniform bore. *J. Fluid Mech.* **95**, 323–345.

Holman, R. A. & Sallenger, A. H. 1993 Sand bar generation: a review of the Duck experiment series. *J. Coastal Res.* **SI 15**, 76–92.

Jansen–Stelder, B. 2000 The effect of different hydrodynamic conditions on the morphodynamics of a tidal mudflat in the Dutch Wadden Sea. *Cont. Shelf Res.* **20**, 1461–1478.

Kirby, R. 1992 Effects of sea level rise on muddy coastal margins. In *Dynamics and Exchanges in Estuaries and the Coastal Zone* (ed. D. Prandle). American Geophysical Union.

Kirby, R. 2000 Practical implications of tidal flat shape. *Cont. Shelf Res.* **20**, 1061–1077.

Komar, P. D. 1998 *Beach Processes and Sedimentation* (2nd edn). Prentice-Hall.

KRONE, R. B. 1993 Sedimentation revisited. In *Nearshore and Estuarine Cohesive Sediment Transport* (ed. A. Mehta). American Geophysical Union.

LE HIR, P., ROBERTS, W., CAZAILLET, O., CHRISTIE, M., BASSOULLET, P. & BACHER, C. 2000 Characterization of intertidal flat hydrodynamics. *Cont. Shelf Res.* **20**, 1433–1459.

LEE, S.-C. & MEHTA, A. J. 1997 Problems in characterising dynamics of mud shore profiles. *J. Hydr. Engng* **123**, 1–11.

NICHOLS, M. M. & BIGGS, R. B. 1985 Estuaries. In *Coastal Sedimentary Environments* (2nd edn) (ed. R. Davis). Springer.

O'BRIEN, D. J., WHITEHOUSE, R. J. S. & CRAMP, A. 2000 The cyclic development of a macrotidal mudflat on varying timescales. *Cont. Shelf Res.* **20**, 1593–1619.

PEREGRINE, D. H. 1972 Equations for water waves and the approximations behind them. In *Waves on Beaches and Resulting Sediment Transport* (ed. R. Meyer). Academic.

PRESS, W. H., TEUKOLSKY, S. A., VETTERLING, W. T. & FLANNERY, B. P. 1992 *Numerical Recipes in Fortran 77* (2nd edn). Cambridge University Press.

PRITCHARD, D. & HOGG, A. J. 2003 Cross-shore sediment transport and the equilibrium morphology of mudflats under tidal currents. *J. Geophys. Res.* (in press).

PRITCHARD, D., HOGG, A. J. & ROBERTS, W. 2002 Morphological modelling of intertidal mudflats: the role of cross-shore tidal currents. *Cont. Shelf Res.* **22**, 1887–1895.

ROBERTS, W., LE HIR, P. & WHITEHOUSE, R. J. S. 2000 Investigation using simple mathematical models of the effect of tidal currents and waves on the profile shape of intertidal mudflats. *Cont. Shelf Res.* **20**, 1079–1097.

RODRIGUEZ, H. N. & MEHTA, A. J. 2001 Modelling muddy coast response to waves. *J. Coastal Res.* **SI 27**, 137–148.

SANFORD, L. P. & HALKA, J. P. 1993 Assessing the paradigm of mutually exclusive erosion and deposition of mud, with examples from upper Chesapeake Bay. *Mar. Geol.* **114**, 37–57.

SANFORD, L. P. & MAA, J. P.-Y. 2001 A unified erosion formulation for fine sediments. *Mar. Geol.* **179**, 9–23.

STANSBY, P. K. & AWANG, M. A. O. 1998 Response time analysis for suspended sediment transport. *J. Hydraul Res.* **36**, 327–338.

VINCENT, S., CALTAGIRONE, J.-P. & BONNETON, P. 2001 Numerical modelling of bore propagation and run-up on sloping beaches using a MacCormack TVD scheme. *J. Hydraul Res.* **39**, 41–49.

WHITEHOUSE, R. J. S. & MITCHENER, H. J. 1998 Observations of the morphodynamic behaviour of an intertidal mudflat at different timescales. In *Sedimentary Processes in the Intertidal Zone* (ed. K. S. Black, D. M. Paterson & A. Cramp). Geological Society, London.

WINTERWERP, J. C. 2002 On the flocculation and settling velocity of estuarine mud. *Cont. Shelf Res.* **22**, 1339–1360.